Experimental Effects on Rapidity Correlations

Warren Li
University of Missouri - St. Louis

Advisor: Dr. W.J. Llope
Wayne State University

August 11, 2016

Abstract

Rapidity correlations were studied to understand the phase diagram of nuclear matter. Data from UrQMD-generated events were used. This model simulates heavy ion collisions at various beam energies. Central collisions of Au nuclei at different beam energies were analyzed using the normalized covariance R_2. This paper discusses how rapidity correlations are affected by experimental effects such as the variation of the collision vertex along the beam pipe, the rapidity window in which the analysis is done, and experimental inefficiencies. It was found that the correlation function is largely unaffected for increasing rapidity widths. Small differences were due to the dependence of correlation on the average rapidity. When the efficiency was applied, similar results were found and the variable remained insensitive to single-particle inefficiencies.

1 Introduction

The QCD phase diagram is not completely understood. For instance, the first-order phase transition and critical point shown in Figure 1 are both speculative. The phase diagram is a function of temperature (T) versus baryochemical potential (μ_B). By colliding heavy ions at relativistic speeds, particle production occurs at high temperatures. This results in a state of matter known as Quark-Gluon Plasma (QGP), where constituent quarks and gluons are free for a brief time. Eventually, particle production and inelastic collisions between particles stop in a process known as chemical freeze-out. This is followed by kinetic freeze-out where all particle momenta are frozen prior to hitting the detector. Understanding the QGP may provide information about the core of neutron stars and the early universe approximately 10 μs after the Big Bang.

Figure 1: QCD phase diagram[1]

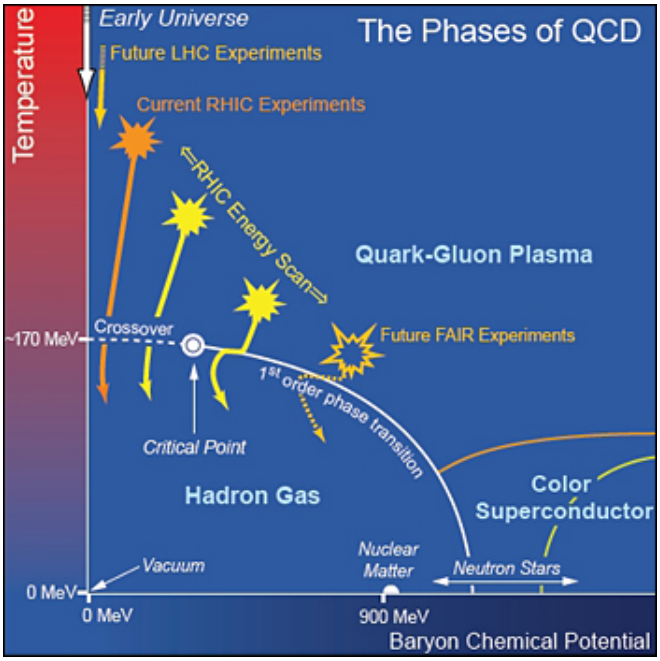

Experiments are carried out at the Solenoidal Tracker (STAR) at Brookhaven National Laboratory's Relativistic Heavy-Ion Collider (RHIC)[2]. There, collisions are performed in a range of beam energies between 7.7-200 GeV. By varying the beam energy, one can "scan" across the x-axis of this diagram since μ_B decreases with increasing energy.

The data in this paper are generated from Ultrarelativistic Quantum Molecular Dynamics (UrQMD)[3], a Monte-Carlo simulation package that models heavy ion collisions. Our goal of the STAR experiment is to search for the speculative phase transition in Figure 1. In phase transitions, fluctuations increase. Thus, the study of the strength of fluctuations and correlations is important for understanding the phase diagram.

The strength of correlations can be evaluated by analyzing a quantity called the covari-

ance:

$$Cov(x, y) = \langle xy \rangle - \langle x \rangle \langle y \rangle \tag{1}$$

If the variables x and y are correlated, which means y increases as x increases, $cov(x, y) > 0$. When $cov(x, y) < 0$, the variables are anti-correlated and y decreases as x increases. A covariance equal to zero signifies no correlation. In this paper, we study a normalized covariance called R_2:

$$R_2 = \frac{\rho_2(y_1, y_2)}{\rho_1(y_1)\rho_1(y_2)} - 1 \tag{2}$$

which has the same behavior as covariance. We investigated how this variable depends on experimental aspects such as the width of the rapidity window, the experimental inefficiencies for measuring the particles, and z-vertex smearing. That is, collisions do not always occur at the center of the detector, and therefore, the dependence on the rapidity of the measurement efficiency is different for every event. This variability could produce additional fluctuations and change the R_2 values.

2 Variables

Collisions are classified by their impact parameter, b, which is the perpendicular distance between the centers of the two nuclei. Collisions with $b \approx 0$ are central or "head-on" collisions, while collisions with larger values of b are peripheral collisions. In a peripheral collision, particles that collide with other particles are called participants, while those that miss are called spectators. For the following data, we have chosen "central" (0-5%) Au+Au collisions, which correspond to impact parameters $0 < b < 3.2$ fm.

The rapidity of a particle is defined as,

$$y = \frac{1}{2} \ln \left(\frac{E + p_z}{E - p_z} \right) \tag{3}$$

where E is the total energy, and p_z is component of the momentum along the beam axis. It is sometimes convenient to use psuedorapidity, which is equal to the rapidity if $m \ll p$ (where m is the mass of the particle):

$$\eta = -\ln \left[\tan \left(\frac{\theta}{2} \right) \right] \tag{4}$$

where θ refers to the angle between the particle 3-vector momentum and the positive z-axis.

Figure 2 outlines the process for generating plots using ROOT[4], a data-analysis framework for C++. First, a multiplicity plot is generated from a Gaussian distribution giving $N_{protons}$/event. Then for each event, a rapidity between -1 to 1 is randomly assigned according to a flat distribution. Pairs of particle rapidities (excluding self-pairs) are plotted to create $\rho_2(y_1, y_2)$, and the tensor product $\rho_1(y_1)\rho_1(y_2)$ is also calculated. Using the definition of R_2 in Equation 2, these 2D histograms are divided, and then 1 is subtracted from each

bin. In such a simulation, one would expect $R_2 = 0$ versus Δy since there cannot be any correlations between the protons when generated this way.

Figure 2: Histograms for randomly-generated rapidities

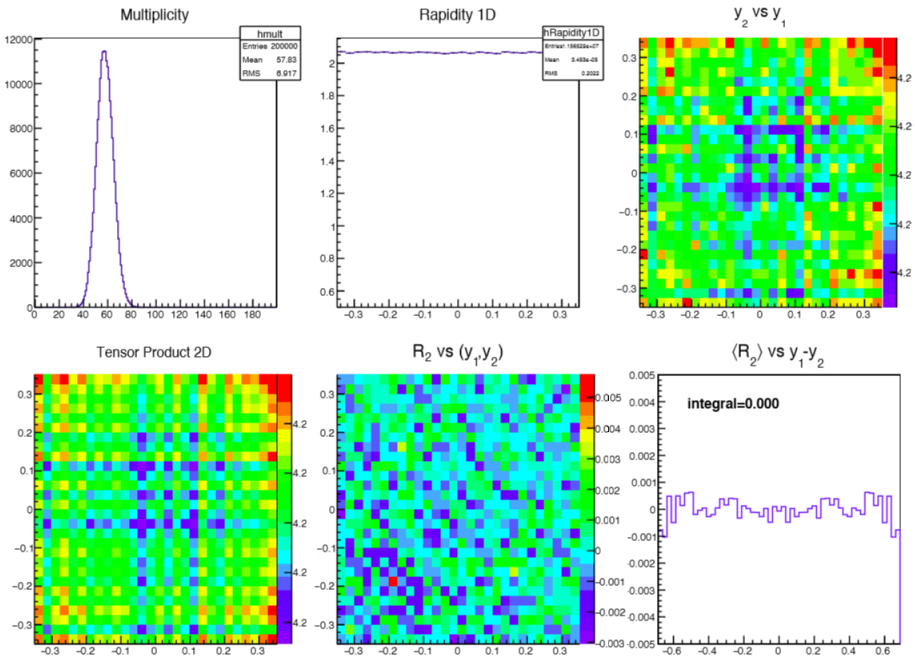

Shown in the upper left of Figure 2 is the multiplicity distribution per event for 200,000 events from 0-5% central collisions from the UrQMD model at 7.7 GeV. The upper middle frame is the rapidity distribution in the range of -0.32 to 0.32 for particles sampled from a flat distribution. Shown in the upper right figure is the numerator of R_2, and the lower left figure is the denominator. The lower middle frame shows R_2, and indeed, the z-axis is centered around zero as expected.

The lower right figure is a diagonally averaged plot of R_2 (the lower middle figure). The diagonal averaging is done as described in Figure 3, the same plot as in the lower right frame of Figure 2. The bins along various Δy values are averaged to produce $\langle R_2 \rangle$ as a function of the rapidity difference $y_1 - y_2$.

When the multiplicities per event are small, this variable is not zero even when there are no correlations. This can be corrected by subtracting a baseline value from all the bins on the right side of Figure 3, which is calculated from the multiplicity distribution in Figure 2. Specifically,

$$R_2^{bs} = \frac{\langle n(n-1) \rangle}{\langle n \rangle^2} - 1 \tag{5}$$

was subtracted to form a corrected $\langle R_2 \rangle - R_2^{bs}$ versus Δy plot.

We now turn to the results from the event generator UrQMD. This model contains all of the hadronic physics processes involved in heavy ion collisions, but does not include the first-order phase transition or critical point. It is however a fairly realistic model and is

Figure 3: Averaging procedure

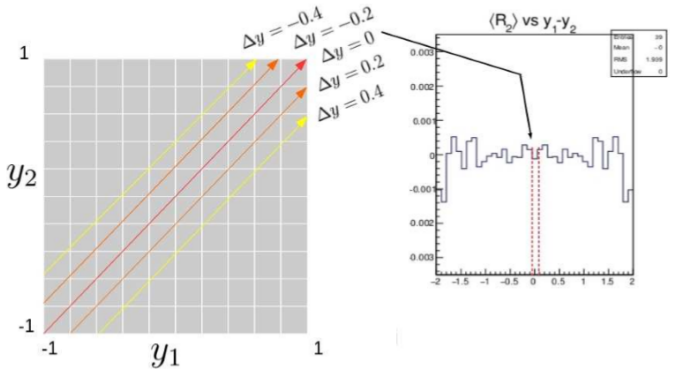

used by many experiments. Figure 4 shows plots for 500,000 UrQMD events at 7.7 GeV. The frames in this plot have the same meaning as Figure 2. However, note that there are strong correlations in the lower middle and right frames. This means that given a proton somewhere in the experiment, it is likely that there is another proton ± 0.7 units of rapidity away. Likewise, the dip near zero means that there is a low probability of encountering a proton with a small Δy nearby.

Figure 5 shows $\langle R_2 \rangle$ versus Δy for 7.7, 27, and 200 GeV for 200,000 events. There is an interesting dependence on the beam energy (μ_B from Figure 1). As the beam energy increases, the (anti)correlations decrease. However, the goal of this analysis is to study experimental effects on the correlations. Therefore, for the remainder of this paper, we concentrate on 7.7 GeV data where there are the strongest correlations.

Figure 4: 7.7 GeV plots

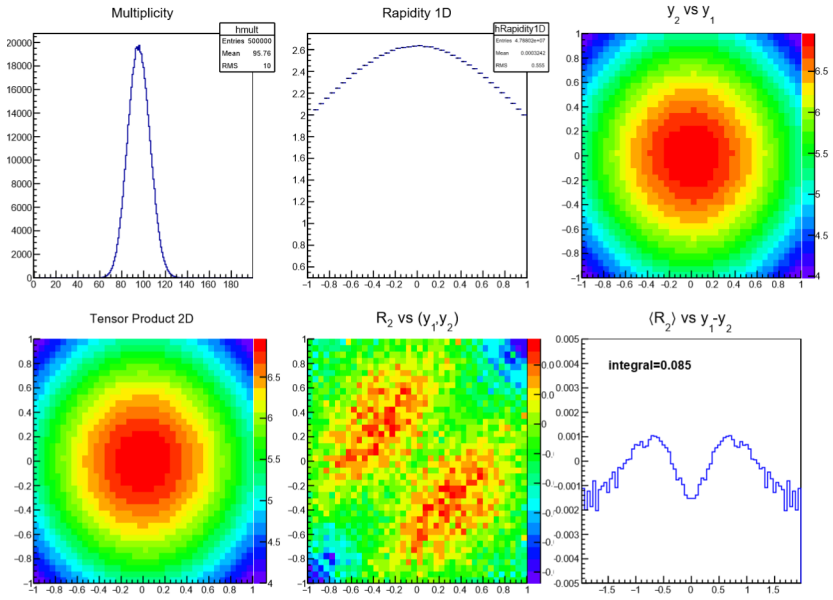

Figure 5: From left to right, 7.7, 27, and 200 GeV

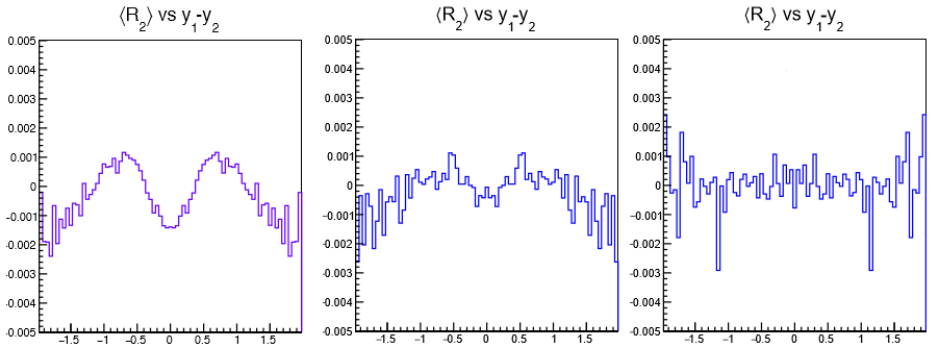

3 Results

In different events, the collision occurs at different locations along the z-axis. Therefore, the experimental acceptance also moves with respect to z. Consequently, it is important to understand where the experiment is as a function of the z-vertex in units of rapidity. Figure 6 shows a diagram of STAR and the relationship between the particle (η_p) and detector (η_d) psuedorapidity for a positive z-vertex value as an example.

Figure 6: Diagram of the STAR detector[5]

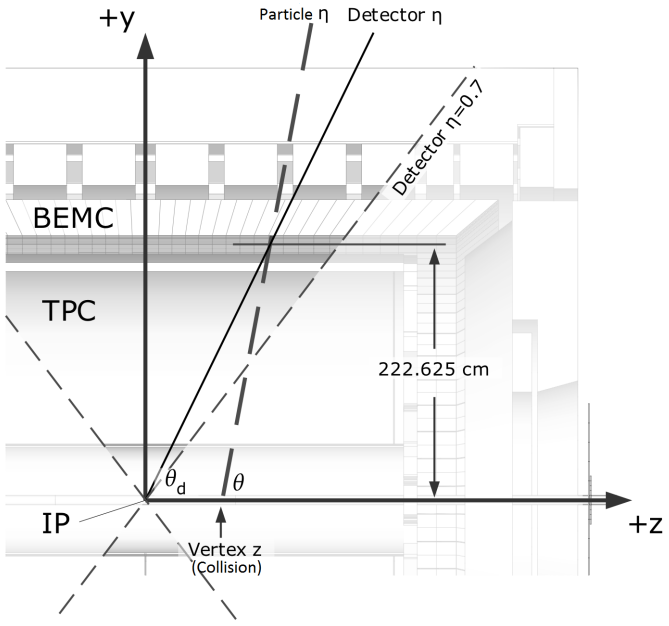

By definition, from η_p, the particle polar angle is obtained by,

$$\theta_p = 2 \arctan\left(e^{-\eta_p}\right), \tag{6}$$

and then the polar angle with respect to the detector is,

$$\theta_d = \arctan\left(\frac{R_d}{z - z_{vtx}}\right), \tag{7}$$

where

$$z = \frac{R_d}{\tan\theta_p}. \tag{8}$$

As an example, if z-vertex is at the center, one will always measure the particles between $-1 < \eta_d < 1$, but as z-vertex moves to the right, $|\eta_d| < 1$ is not measured with the same number of pad rows and the efficiency of those tracks decrease. Because of this experimental effect, the region with the highest efficiency in rapidity or psuedorapidity changes event by event. To understand this, we begin by understanding the relationship between psuedorapidity and particle rapidity.

Shown in Figure 7 is the particle rapidity versus psuedorapidity for protons, kaons, and pions. For pions, the lightest of the three particles, the graphs are more diagonal and psuedorapidity and rapidity are nearly identical. For heavier particles however, these two quantities diverge depending on the transverse momentum p_T, as labeled. The greatest efficiency occurs when $|\eta_d| < 1$. The range in rapidity that one can measure with high efficiency depends on the width of the z-vertex cut. Thus, we tabulated the maximum values for y with good detector efficiencies for a displaced z-vertex in Table 1.

Figure 7: Particle rapidity against psuedorapidity for protons, kaons, and pions and $z_{vtx} = 0$

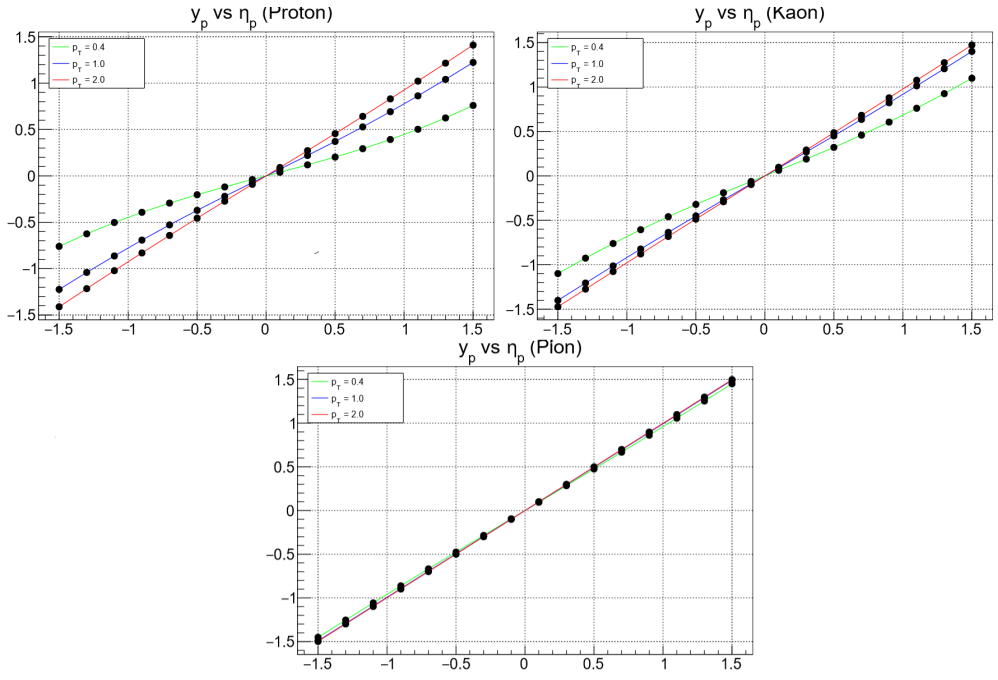

Given this information about the relationships between η_p, y_p, and η_d, it is then relevant to study how the strength of the correlations in the UrQMD events depends on the y

Table 1: y ranges for various p_T with the condition that $|\eta_d| < 1$ at $z_{vtx} = 0$ and 30 cm

$z_{vtx} = 0$, $\eta_p = 1$				$z_{vtx} = 30$, $\eta_p = 0.899$			
p_T	y_p min	y_p max	Particle	p_T	y_p min	y_p max	Particle
0.4	-0.447	0.447	p^+	0.4	-0.499	0.392	p^+
1.0	-0.777	0.777	p^+	1.0	-0.858	0.691	p^+
2.0	-0.926	0.926	p^+	2.0	-1.016	0.830	p^+
0.4	-0.683	0.683	k^+	0.4	-0.756	0.605	k^+
1.0	-0.918	0.918	k^+	1.0	-1.008	0.822	k^+
2.0	-0.977	0.977	k^+	2.0	-1.070	0.878	k^+
0.4	-0.960	0.960	π^+	0.4	-1.051	0.861	π^+
1.0	-0.993	0.993	π^+	1.0	-1.087	0.893	π^+
2.0	-0.998	0.998	π^+	2.0	-1.092	0.897	π^+

window used for the analysis. This is shown in Figure 8. In each frame of this figure, the same experimental events are used. However, the width of the rapidity window is gradually increased in each frame. The comparison of these different windows is shown in the bottom right frame.

One sees that the correlation function for $\langle R_2 \rangle$ is similar when proceeding to larger rapidities. The slight difference between these values is caused by the dependence of the correlation on the average rapidity, which can also increase when increasing the Δy window. This is illustrated in Figure 9. As the rapidity window expands, which is shown by the square boxes, both Δy and $\langle y \rangle$ increase. A small Δy at mid average rapidity is not the same as small Δy at large average rapidity. Since the correlations can depend on $\langle y \rangle$, one would not expect the plots to be identical. It is clear however that the effect on $\langle R_2 \rangle$ from reasonably sized Δy windows is rather small.

Figure 8: $\langle R_2 \rangle$ vs Δy for various y-widths

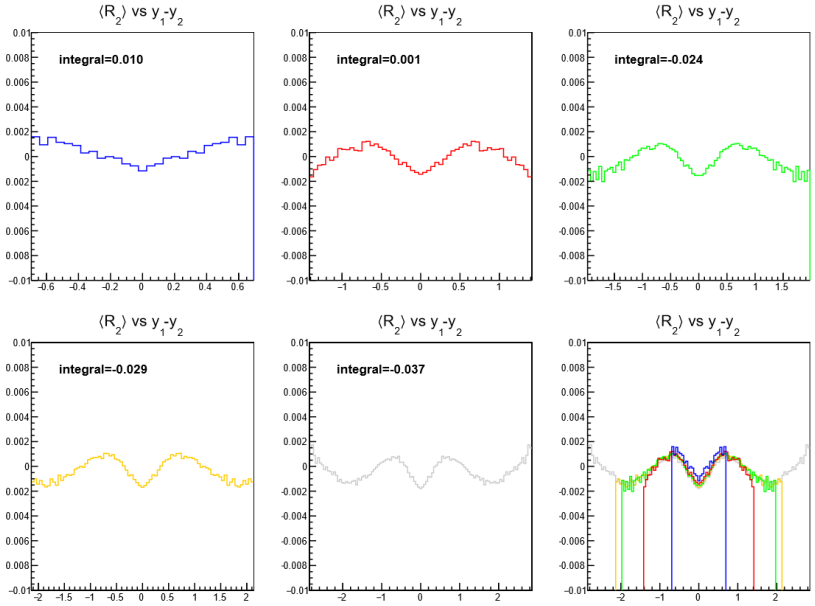

Figure 9: When increasing the width on Δy allowed in the analysis, one also increases $\langle y \rangle$

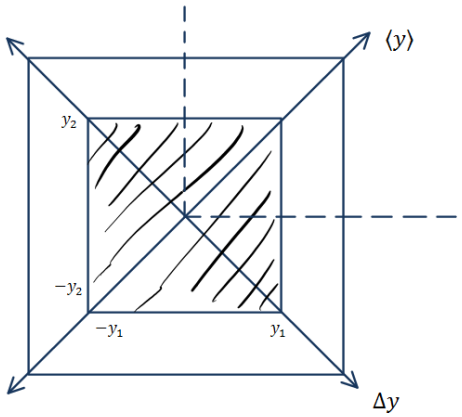

So far, events were studied from a model where every particle produced in a collision is measured. In reality, this is not the case. Modern detectors cannot measure every particle emitted due to cracks in the detector (for example, to allow for signal cables) and because particles with low p_T spiral in the magnetic field. This means that slowly-moving particles have low efficiencies. We are therefore interested in understanding how experimental efficiencies impact the $\langle R_2 \rangle$ values.

Note that according to Equation 2, the variable studied is a two-dimensional distribution divided by the tensor product of two one-dimensional distributions. Therefore, the values of R_2 go as,

$$\frac{\epsilon^2}{\epsilon * \epsilon} = 1 \tag{9}$$

so R_2 is expected to be insensitive to the single-particle inefficiencies. We now test this with UrQMD events.

For every particle that is emitted by the event generator, a random number is thrown. This number is then compared to tabulated efficiency curves as a function of p_T, y, and centrality. If the efficiency is larger than the random number, the particle is measured. Otherwise, the particle is discarded. This effectively applies the inefficiencies to the UrQMD simulated events.

Shown in Figure 10 is the value of $\langle R_2 \rangle$ for three cases: a perfect detector (lower left), a p_T cut applied (upper right), and a parameterized plot as a function of p_T, y, and centrality (upper left). The effect of the efficiency on the variable is small as expected because the single-particle efficiencies divide out. Slight differences seen are due to the fact that the parameterized efficiency effectively includes a rapidity cut, which effectively narrows the y-window and results in a similar effect as described previously in Figure 9.

Figure 10: Comparison of experimental acceptance to a perfect detector

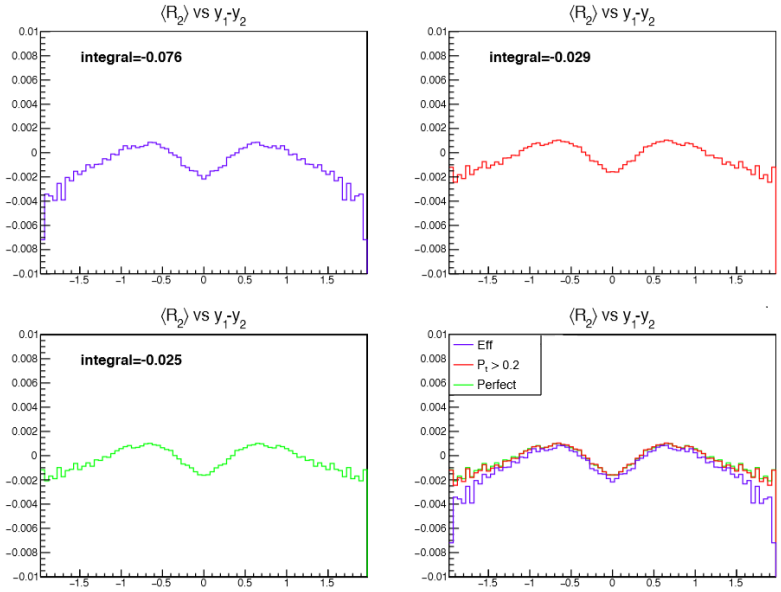

4 Conclusion

The QCD phase diagram is speculative. However, by changing beam energy, one can "scan" across the x-axis of the diagram. In phase transitions, fluctuations increase. Thus, the study of the strength of fluctuations and correlations is important for understanding the phase diagram. In this study, experimental effects on two-particle correlations were analyzed using the normalized covariance R_2. We started by understanding the relationship between particle psuedorapidity and rapidity given a z-vertex value. These two quantities do not agree for heavy particles. The maximum values for y with good detector efficiencies for displaced z-vertex values were tabulated.

Next, we studied how the strength of correlation in UrQMD events depends on the width of the y window used for the analysis. It was shown that the correlation function for $\langle R_2 \rangle$ is largely unchanged when proceeding to larger rapidity windows. The slight difference between values were caused by the dependence of correlation on the average rapidity. Finally, inefficiencies were applied. We find that single-particle efficiencies divide out, and slight differences seen are due to the fact that parameterized efficiency includes the dependence of the efficiency on the rapidity, which effectively narrows the y-window.

5 Acknowledgments

This program was funded by the National Science Foundation (NSF) under grant PHY-1460853. Thanks to Professors Petrov and Cinabro for running Wayne State's Research Experience for Undergraduates (REU) program. Thank you to my advisor Dr. Llope for his time, suggestions, and insight. Lastly, I want to thank postdoctoral fellow Ayeh Jowzaee for many helpful discussions.

6 References

[1] "How Low Can RHIC Go?" Brookhaven National Laboratory. 22 July 2010.

[2] "The STAR Experiment". 13 May 2016. `https://www.star.bnl.gov`

[3] "The UrQMD Model." `https://urqmd.org`

[4] "ROOT-Data Analysis Framework." 2016. `https://root.cern.ch`

[5] "Jet η and detector η." STAR Images: Brookhaven National Laboratory.